

# Confinement effects upon the separation of structural transitions in linear systems with restricted bond fluctuation ranges

Tomas Koci<sup>1,\*</sup> and Michael Bachmann<sup>1,2,3,†</sup><sup>1</sup>*Soft Matter Systems Research Group, Center for Simulation Physics, The University of Georgia, Athens, Georgia 30602, USA*<sup>2</sup>*Instituto de Física, Universidade Federal de Mato Grosso, Cuiabá (MT), Brazil*<sup>3</sup>*Departamento de Física, Universidade Federal de Minas Gerais, Belo Horizonte (MG), Brazil*

(Received 13 April 2015; published 20 October 2015)

By means of advanced parallel replica-exchange Monte Carlo methods we examine the influence of elasticity and confinement on the structural transitions of linear systems with restricted bonded interaction. For this purpose, we adopt a model for coarse-grained flexible polymers of finite length in the dilute regime. Hyperphase diagrams are constructed using energy-dependent canonical quantities to demonstrate the effects of the changes in the range of the confined interaction on the liquid and solid structural phases. With increasing bonded interaction range we observe the disappearance of the liquid phase and the fusion of the gas-liquid (or  $\Theta$ ) and the liquid-solid transitions. One of the most remarkable features, the liquid-gas transition, changes from second to first order if the confined interaction range exceeds a threshold that separates polymeric from nonpolymeric systems. The notoriously difficult sampling of the entropically suppressed conformations in the region of very strong first-order transitions is improved by using multiple Gaussian modified ensembles.

DOI: [10.1103/PhysRevE.92.042142](https://doi.org/10.1103/PhysRevE.92.042142)

PACS number(s): 05.70.Fh, 64.60.De, 64.70.-p, 82.35.Lr

## I. INTRODUCTION

Polymers of mesoscopic size are complex objects and their structural behavior depends sensitively on the mutual interaction between the monomers and the influence of the thermal environment. For the understanding of biomolecular function and chemico-physical material properties of biopolymers and synthetic polymers, respectively, studies of their thermodynamic structural phases are of utmost relevance. A completely different system, atomic clusters with long-range interactions behave like a confined system as well. Therefore, it is no surprise that the freezing behavior of atomic clusters is very similar to that of flexible, elastic polymers [1].

Hence, it is an interesting and fundamental problem to model the interpolation between these systems and to study the influence of bond confinement upon the formation and stability of structural phases by employing a simple bead-spring model.

Because of the immense difficulties associated with the mathematical and experimental investigation of finite polymers, computer simulations of models that capture the cooperative features of structure formation are currently the only way to address the interplay of entropic and energetic properties of entire classes of confined systems systematically [2].

Within the past two decades, thanks to the availability of vast computational resources and substantial advances in methodological development, there has been enormous progress in unraveling thermodynamic properties of structural phases. In particular, the growing necessity to understand protein folding also boosted investigations of cooperative conformational phase behavior of small linear polymers, which can be described by rather simple models. Coarse-grained polymer and protein models have been proven to be useful for the investigation of collapse, freezing, or folding of individual macromolecules such as proteins [3–12] and polymers [1,13–23].

Generic features of polymer adsorption on substrates [24–37] and the aggregation of macromolecules [38–41] can also be described adequately by means of simplified models.

On the other hand, the investigation of features of small atomic clusters has found similar attention. While most studies focused on the identification of structural ground-state properties, the thermodynamic transition behavior has been of interest as well [42–47]. Comparisons between thermodynamic properties of the freezing behavior of clusters and polymers have been performed recently [1,48]. In all cases, finite-size effects such as solid-solid transitions induced by atomic reordering on the surface of the cluster matter and have to be incorporated into the interpretation of the transition behavior.

Computer simulations using Monte Carlo algorithms in generalized ensembles, such as the replica-exchange (parallel tempering) method [49–52], simulated tempering [53,54], and also multicanonical [2,55–60] and Wang-Landau sampling [61–63], are particularly feasible and efficient for thermodynamic studies of structural polymer phases. Alternatively, for studies of lattice polymers, chain-growth methods turned out to be most appropriate [7–9,15,64]. The intricate impact of finite-size effects on the thermodynamic phase behavior requires careful statistical analyses beyond conventional canonical methods that typically do not allow for a unique identification of transition points in finite systems [2,8]. On the contrary, general methods such as analyses of inflection points in the microcanonical temperature curve [65], which is based on microcanonical thermodynamics [66], autocorrelation times [67], and Fisher partition function zeros [68], have been employed successfully recently [69–71].

One important aspect in the study of structural transitions in polymer systems is the influence of model (“material”) and environmental parameters upon the processes that lead to structure formation and the conformations themselves. In recent studies, the effect of the interaction range between nonbonded monomers has been addressed systematically [19,20,23]. It has been found that for sufficiently short interaction ranges,

\*koci@smsyslab.org

†bachmann@smsyslab.org; <http://www.smsyslab.org>

it is possible for the polymer to fold directly from random-coil structures (i.e., the gas phase) into solid and compact conformations. Under these conditions, no globular (or liquid) phase is present.

In this paper, we investigate the influence of bond confinement range upon the structural phases and the transition behavior of a flexible chain of bonded beads. The variation of the bond extension range allows us to bridge the gap between self-interacting polymers with stiff bonds (such as proteins) and bead-spring chains (elastic polymers) with bonds so floppy that the system behaves similarly to a gas of interacting particles.

For this purpose, we have performed extensive replica-exchange Monte Carlo simulations in extended multiple Gaussian modified ensembles [72], which help improve the efficiency of parallel tempering simulations near first-order transitions. Systematic studies of the structural phases in the space of the bond confinement parameter were made possible by employing standard canonical analyses of fluctuations in macroscopic thermodynamic quantities and also by careful analysis of the nature of inflection points in the microcanonical temperature curve [2,65]. The latter method allows for the identification of the order of structural transitions in finite systems.

The paper is organized as follows: In Sec. II, we introduce the model for flexible elastic linear chains used in our study, describe the generalized-ensemble methods employed, and review the microcanonical statistical analysis of structural transitions in finite systems. The results of the simulations are presented in Sec. III, where the changes of the transition behavior of the linear chains upon variation of the confinement range are discussed on the basis of canonical and microcanonical statistical analyses. The paper is concluded by a summary in Sec. IV.

## II. FLEXIBLE BEAD-SPRING SYSTEMS WITH VARIABLE BOND CONFINEMENT RANGE

In the following, we introduce the model for flexible bead-spring systems, the simulational methodologies, and the methods of statistical analysis that enabled us to study the entire space of confinement parameters, in which the structural phase transition behavior of the system changes.

### A. Standard model of elastic chains

In this study, we employ a generic model of a bead-spring model that has been introduced originally for investigations of general properties of single, elastic, flexible, linear homopolymer chains. Due to the similarity in the transition behavior of atomic clusters and polymers, however, the scope of this model can be extended to investigate effects of bond confinement as well. As such, this model allows for the interpolation of systems ranging from polymers to an almost unconfined gas of atoms.

Consider a chain with  $N$  beads (atoms or monomers). A pair of beads  $i$  and  $j$  ( $i, j \in [1, N]$ ,  $i \neq j$ ) with relative distance  $r_{ij}$  interacts via a truncated and shifted Lennard-Jones potential

$$U_{\text{LJ}}^{\text{trunc}}(r_{ij}) = \begin{cases} U_{\text{LJ}}(r_{ij}) - U_{\text{LJ}}(r_c), & r_{ij} \leq r_c, \\ 0, & r_{ij} > r_c, \end{cases} \quad (1)$$

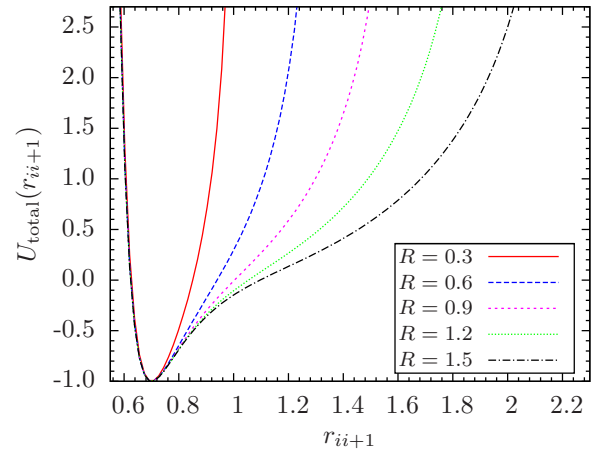


FIG. 1. (Color online) Behavior of the combined bond potential  $U_{\text{total}}(r_{ii+1}) = U_{\text{LJ}}(r_{ii+1}) + U_{\text{FENE}}(r_{ii+1})$  for different values of the effective confinement range  $R$ .

where

$$U_{\text{LJ}}(r_{ij}) = 4\epsilon \left[ \left( \frac{\sigma}{r_{ij}} \right)^{12} - \left( \frac{\sigma}{r_{ij}} \right)^6 \right], \quad (2)$$

with the energy scale set to  $\epsilon = 1$  and the length scale to  $\sigma = r_0/2^{1/6}$ , where  $r_0 = 0.7$  is the location of the minimum potential. We select a cut-off radius  $r_c = 2.5\sigma$  such that  $U_{\text{LJ}}(r_c) \approx -0.0163169\epsilon$ .

The bonds between the adjacent beads are represented by the anharmonic finitely extensible nonlinear elastic (FENE) potential [73–75], which we use here in modified form

$$U_{\text{FENE}}(r_{ii+1}) = -\frac{K}{2} R_0^2 \ln \left[ 1 - \left( \frac{r_{ii+1} - r_0}{R} \right)^2 \right]. \quad (3)$$

We set  $K = 40$  and  $R_0 = 0.3$  [23]. The parameter  $R$  controls the effective confinement range of the bonds, whereas the energy scale is kept constant. The qualitative behavior of the combined bond potential for different values of  $R$  is shown in Fig. 1. The confinement range increases with  $R$ , i.e., by changing  $R$  in a wide range of values ( $R \in [0.3, 90]$ ), we systematically investigate an entire class of systems interpolating between the limits of stiff polymers ( $R \rightarrow 0$ ) and, effectively, a gas of nonbonded Lennard-Jones particles (“noble gas”), for which  $R \rightarrow \infty$ .

In our simulations, the system was constrained inside of a steric sphere at a constant density of 0.001 particles per unit volume, in which case the diameter of the sphere is larger than the length of the fully extended chain. Under these conditions, we consider the system to be highly dilute.

The total energy of a polymer chain of length  $N$  in a conformation  $\mathbf{X} = (\vec{r}_1, \dots, \vec{r}_N)$  is given by

$$E(\mathbf{X}) = \sum_{i < j}^N U_{\text{LJ}}^{\text{trunc}}(r_{ij}) + \sum_{i=1}^{N-1} U_{\text{FENE}}(r_{ii+1}). \quad (4)$$

The results presented in this paper are compared for classes of chains with  $N = 13$  and 30 beads. For verification purposes, we have also studied systems with up to 55 beads, which, for

this kind of systematic study that covers the entire state space, represents the limit of currently feasible simulations.

### B. Replica-exchange simulations in multiple canonical and Gaussian modified ensembles

For our simulation, we have used replica-exchange Monte Carlo (parallel tempering) [49–52], extended to multiple Gaussian modified ensembles (MGME) [72]. In parallel tempering,  $M$  replicas of the system are simulated in parallel at inverse temperatures in the interval  $\beta \in [0.5, 50]$ . The conformations in an individual temperature thread are updated using random single-bead displacements with the acceptance probability given by the Metropolis criterion

$$A(\mathbf{X}_{\text{old}} \rightarrow \mathbf{X}_{\text{new}}) = \min(1, e^{-\beta[E(\mathbf{X}_{\text{new}}) - E(\mathbf{X}_{\text{old}})]}). \quad (5)$$

Periodically, an exchange of conformations between adjacent replicas  $i$  and  $j$  is proposed with the acceptance probability

$$A(\mathbf{X}_i \leftrightarrow \mathbf{X}_j; \beta_i, \beta_j) = \min(1, e^{[\beta_j - \beta_i][E(\mathbf{X}_j) - E(\mathbf{X}_i)]}). \quad (6)$$

In principle, this allows each replica to traverse the entire simulated temperature range which would decrease the auto-correlation time and increase sampling efficiency. However, the performance of this method rapidly decreases near first-order transitions with high free-energy barriers due to entropic depletion of energetic states. As Fig. 2 shows, this issue is encountered in elastic chain systems with large confinement range or gaslike systems (large  $R$  values).

An alternative scheme that offers improved sampling in strongly first-order transition regions is based on the combination of parallel tempering with the MGME method [72]. In a single Gaussian modified ensemble (GME) at inverse temperature  $\beta$ , the probability of a state  $\mathbf{X}$  with energy  $E$  is given by

$$P_{\text{GME}}(\mathbf{X}) \sim e^{-\beta E(\mathbf{X}) - [E(\mathbf{X}) - E_G]^2 / \Delta E_G^2}, \quad (7)$$

where  $E_G$  and  $\Delta E_G$  are the center and the width of the Gaussian, respectively. Strong first-order transitions with bimodal energy distributions typically require several over-

lapping GME ensembles to cover the relevant energy range as shown in Fig. 2 for a 30mer with  $R = 30$  at the  $\Theta$  transition temperature. The acceptance probability for the exchange of conformations  $\mathbf{X}_i, \mathbf{X}_j$  between neighboring GME ensembles at inverse temperature  $\beta$  is

$$A(\mathbf{X}_i \leftrightarrow \mathbf{X}_j) = \min(1, e^{\Delta G}), \quad (8)$$

where

$$\Delta G = \frac{(E_i - E_{G,j})^2 - (E_j - E_{G,j})^2}{\Delta E_{G,j}^2} - \frac{(E_j - E_{G,i})^2 - (E_i - E_{G,i})^2}{\Delta E_{G,i}^2}. \quad (9)$$

The resultant energy distribution of this combined MGME ensemble is nearly flat and the Monte Carlo sampling of the entropically suppressed region is enhanced. The sampling can be further improved by combining the MGME method with parallel tempering, hence allowing for exchanges between GME ensembles at different temperatures.

In our simulations, the typical number of replicas used was  $M = 80$ . A replica exchange update was attempted every 100 Monte Carlo sweeps. The acceptance rate for Metropolis updates in each thread was about 40–60%. Replica exchange was accepted at an average rate exceeding 20%. The total number of sweeps totaled  $5 \times 10^8$ . The simulations were carried out on a two-dimensional mesh of temperatures and  $E_G$  values in the first-order transition region. On average 10 different values of  $E_G$  were used per temperature thread.

### C. Microcanonical analysis

As a result of the replica-exchange simulations, we obtain canonical energy histograms  $h(E; \beta_i)$  for the inverse temperatures  $(\beta_1, \beta_2, \dots, \beta_N)$ . Each histogram is a preliminary estimate for the density of states  $g_i(E) \sim h(E; \beta_i) \exp(\beta_i E)$ , up to an unknown constant. Individual histograms cover only that part of the energy space with sufficient accuracy, which is relevant for the canonical ensemble at  $\beta_i$ . These partial estimators can be conveniently combined via the iterative multiple-histogram reweighting method [76,77] to yield an estimator of the density of states that covers the entire energy range of interest.

The microcanonical entropy is the central quantity for the discussion of phase transitions, and it is based on the density of states. It is given by

$$S(E) = k_B \ln g(E). \quad (10)$$

We introduce the inverse microcanonical temperature as the change in the microcanonical entropy caused by a variation in energy

$$\beta(E) = \frac{dS(E)}{dE}. \quad (11)$$

Unlike its canonical counterpart—the heat-bath temperature—the microcanonical temperature is an inherent property of the system. As such, it contains all the information about the interplay of entropy and energy and can be used to locate and classify all structural transitions of the system. In fact, a transition occurs when  $\beta(E)$  responds least sensitively

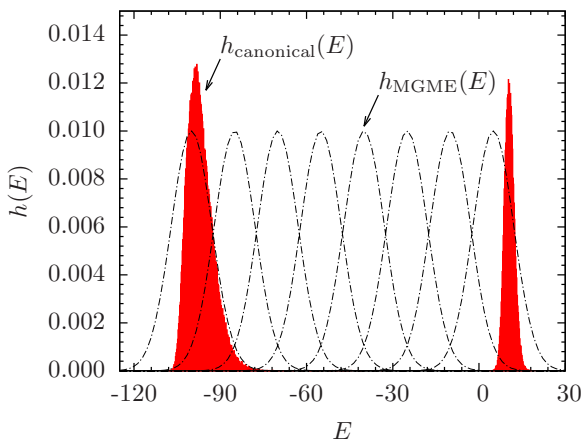


FIG. 2. (Color online) Canonical and MGME energy histograms for a 30mer with  $R = 30$ , exhibiting a strong first-order-like  $\Theta$  transition. The canonical histogram is clearly bimodal while the MGME histograms are all of unimodal shape.

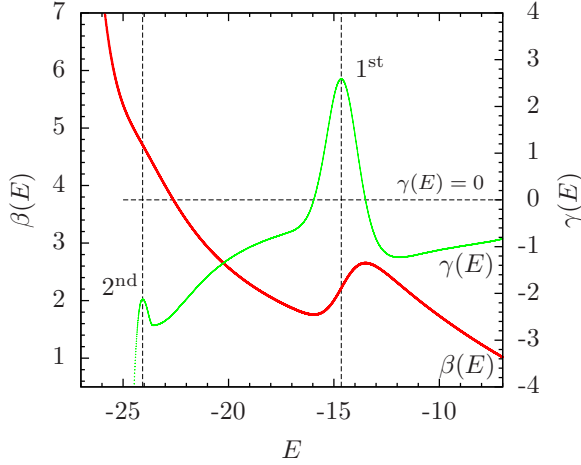


FIG. 3. (Color online) Microcanonical inflection-point analysis of the inverse microcanonical temperature  $\beta(E)$ . The negative-valued peak in the derivative  $\gamma(E) = d\beta(E)/dE$  at  $E \approx -24$  corresponds to a *second-order-like* transition. The positive-valued peak at  $E \approx -15$  indicates a *first-order-like* transition.

to changes in  $E$ . This is embodied by the inflection-point analysis method [2,65]. In this scheme, the convex-to-concave inflection points of  $\beta(E)$  locate an energetic transition point between ensembles of macrostates that can be crossed by a change in energy. We call these ensembles “phases” (sometimes referred to as pseudophases or structural phases), because this microcanonical behavior also remains valid in the thermodynamic limit. If we introduce  $\gamma(E) = d\beta(E)/dE$ , a transition is defined to be of *first order* if  $\gamma(E)$  has a positive peak value at the inflection point. In case the peak value is negative, the transition is classified as of *second order*. This is schematically depicted in Fig. 3. Based on the principle of minimal sensitivity and Ehrenfest’s original idea of characterizing the order of a transition by the free-energy derivative at which a discontinuity occurs, one can likewise introduce a hierarchy of higher-order transitions microcanonically. However, in order to keep the terminology simple, we will denote all transitions beyond first order as *second-order transitions* throughout the paper.

### III. RESULTS

In this section, we investigate the influence of the confinement parameter  $R$  on the structural transitions in elastic chains of lengths  $N = 13$  and  $30$  in the dilute regime. For this purpose, we first perform a conventional canonical statistical analysis of fluctuating quantities and compare with results of a corresponding microcanonical analysis.

#### A. Canonical statistical analysis of energetic and structural fluctuations

For the identification of transition points, we first consider the changes in the thermodynamic behavior of energetic and structural canonical fluctuation quantities. The transition behavior is compared for various values of the confinement parameter  $R$ . This analysis enables us to construct a structural

hyperphase diagram. Differences in the overall generic transition behavior are discussed for two system sizes ( $N = 13, 30$ ).

The statistical fluctuation of a thermodynamic quantity  $O$  is suitably defined by the temperature derivative of its expectation value

$$\langle O(\mathbf{X}) \rangle(T) = \frac{1}{Z(T)} \int \mathcal{D}\mathbf{X} O(\mathbf{X}) e^{-E(\mathbf{X})/k_B T}, \quad (12)$$

where  $\mathcal{D}\mathbf{X}$  is the integral measure in the space of all polymer conformations  $\mathbf{X}$  and

$$Z(T) = \int \mathcal{D}\mathbf{X} e^{-E(\mathbf{X})/k_B T} \quad (13)$$

is the partition function of the canonical ensemble of these structures at the canonical (heat-bath) temperature  $T$ . Thus, changes in the monotonous behavior of

$$\frac{d}{dT} \langle O(\mathbf{X}) \rangle(T) = \frac{1}{k_B T^2} [\langle O(\mathbf{X}) E(\mathbf{X}) \rangle(T) - \langle O(\mathbf{X}) \rangle(T) \langle E(\mathbf{X}) \rangle(T)] \quad (14)$$

indicate pronounced thermal activity of the system. The most common and easiest accessible quantity in Monte Carlo simulations is the specific heat, which represents the fluctuations of energy. In this case  $O = E$  and

$$c_V(T) = \frac{1}{N} \frac{d}{dT} \langle E(\mathbf{X}) \rangle(T).$$

A structural quantity, routinely used for scaling analyses of the  $\Theta$  transition of chain collapse, is the radius of gyration, which is defined by

$$r_{\text{gyr}}(\mathbf{X}) = \sqrt{\frac{1}{N} \sum_{i=1}^N (\mathbf{x}_i - \mathbf{x}_{\text{com}})^2}, \quad (15)$$

where  $\mathbf{x}_{\text{com}} = \sum_{i=1}^N \mathbf{x}_i / N$  is the center-of-mass location of the conformation.

The thermal fluctuations of the energy (specific heat) and of the radius of gyration of 13mers and 30mers are shown in Figs. 4 and 5, respectively, for different values of bond confinement ranges  $R$ . Generally, peaks and “shoulders” in these quantities indicate locations of structural transitions. The generic transitions of elastic chains are the  $\Theta$  collapse transition that separates the gaslike phase of random-coil conformations from the liquid, collapsed globular phase and the freezing transition from the globular into the solid “crystalline” phase [1,18]. Previous studies have shown that both transitions merge if *nonbonded* interactions are extremely short-ranged [19,20,23].

However, a similar behavior is observed in systems with extremely large bond confinement ranges. Whereas, with increasing values of  $R$ , the low-temperature signal in the specific-heat curves in Figs. 4 and 5 (which, for example, for  $R = 3.0$  is still clearly associated with the freezing transition) shifts only slightly to lower temperatures, the  $\Theta$  transition signal drops significantly and finally merges with the freezing transition at  $R \sim 30$ . Whether the freezing and  $\Theta$  transitions remain well separated for all values of  $R < 30$  cannot be unambiguously determined by inspection of the canonical fluctuation quantities, in particular since for  $R > 15$  the freezing transition signal turns into a shoulder on the

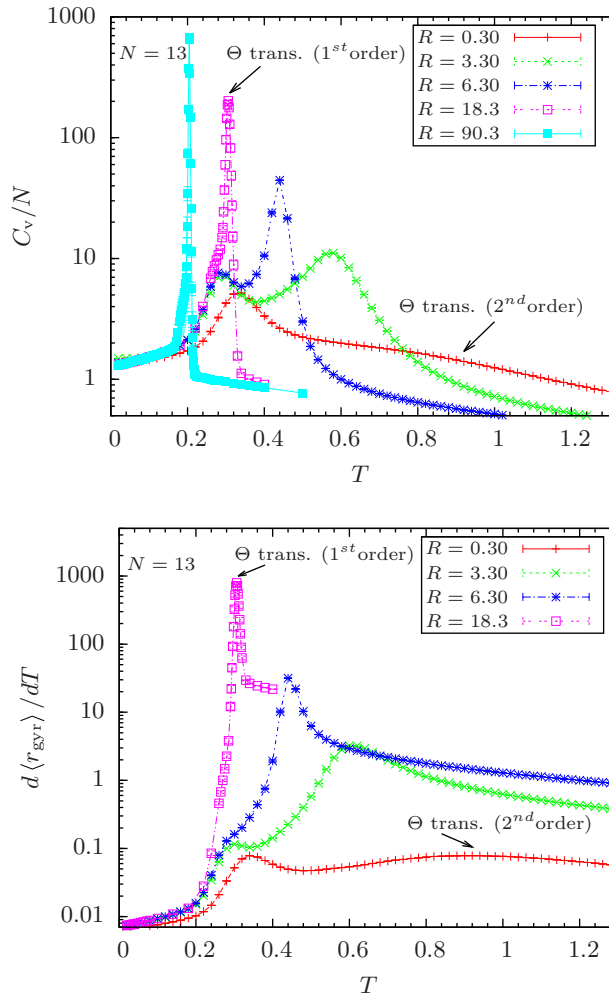


FIG. 4. (Color online) Specific heat and the thermal fluctuations of the radius of gyration for 13mers parametrized by the bond elasticity parameter  $R$ .

low-temperature flank of the more dominant  $\Theta$  transition peak. We will provide evidence for the separation of the transitions with the methods of microcanonical analysis in the next section.

The general freezing transition behavior does not change noticeably until its merger with the  $\Theta$  transition. This is plausible since the freezing transitions are driven mainly by the Lennard-Jones pair interactions between bonded and nonbonded monomers that optimize the icosahedral-like conformations in the solid phase. Therefore, this transition is not significantly affected by the modifications in the bond elasticity.

In the solid phase, the “magic” 13mer possesses a perfect icosahedral shape [1,18], whereas the 30mer forms amorphous structures. The energy histograms of the 13mer exhibit bimodal shapes near the freezing transition point for values of  $R < 30$ , suggesting a first-order-like transition of the finite system.

The “liquid-solid” transition of the 30mer resembles a “liquid-liquid” transition, since the compact globular conformations are difficult to distinguish from the amorphous solid structures. Nonetheless, the transition signal is clearly

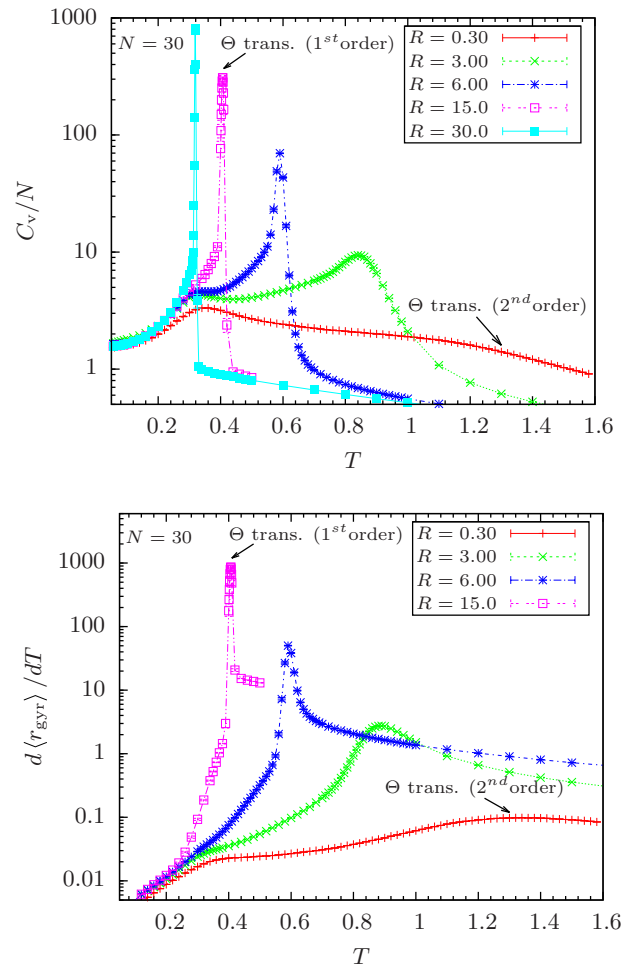


FIG. 5. (Color online) Same as Fig. 4, but for 30mers.

visible and the unimodal shape of the canonical energy histograms (not shown) in this region of  $R$  space indicates a second-order-like transition.

More striking is the dramatic change of the characteristic features of the  $\Theta$  transition. As expected, for  $R \sim 0.3$ , the transition is still *second-order-like* [78,79]. In the specific heat-curves in Figs. 4 and 5 it is clearly visible that with increasing values of  $R$ , the shoulders indicating the  $\Theta$  transitions turn into distinct peaks which rapidly become narrower and more pronounced as they shift to lower temperatures. For values of  $R > 4.5$ , the canonical energy histograms obtained at the transition temperature are no longer unimodal, which suggests that the  $\Theta$  transition becomes *first-order-like*. This can be seen nicely in Fig. 6, where energy histograms for the 13mer with  $R = 15$  at temperatures near the  $\Theta$  transition point are shown. For  $T = 0.33$ , the bimodal shape is clearly visible. The phase separation between gas and liquid is unusual for a polymer and indicates that for  $R = 15$  the particles in the system are quasifree and behave rather like a loosely confined interacting gas, because bond crossings are possible. The disappearance of the two distinct transition signals for  $R > 30.0$  marks the end of existence of a separate liquid phase. This behavior is similar for both systems sizes studied and might be universal. However, the strikingly prominent signals for the  $\Theta$  transition

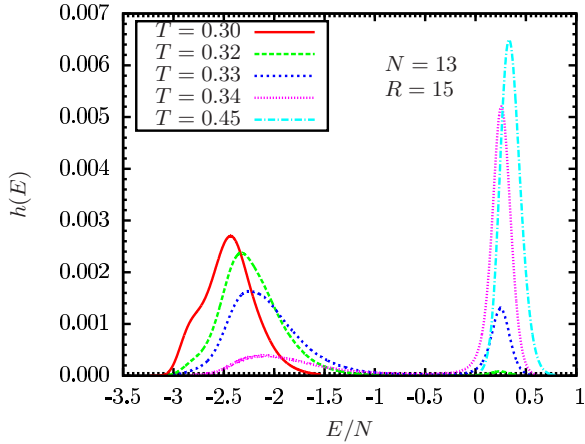


FIG. 6. (Color online) Energy histograms of the 13mer with  $R = 15$  at several temperatures near the  $\Theta$  point.

and the disappearance of the liquid phase are limited to the dilute regime and would not be observed at higher particle densities [80,81].

It should be mentioned that the phase separation becomes substantially stronger for larger  $R$  values, as well as the interfacial surface tension due to the radical entropic depletion in the energetic gap region (cf. the example shown in Fig. 2 for the 30mer with  $R = 30$ ).

With the transition temperatures obtained from the peaks in the canonical quantities we construct structural phase diagrams parametrized by the temperature  $T$  and the confinement parameter  $R$ . For both system sizes, near the unmodified values of  $R$ , we observe three distinct structural phases. The high-temperature curves in Fig. 7 represent the  $\Theta$  transition lines, at which the expanded coils in the gas phase collapse into the compact but disordered globular states in the liquid phase. The pink (patterned) and blue (solid) portions of the  $\Theta$  transition line indicate the regions in which the transition is second-order-like and first-order-like, respectively. The merging of the freezing and the  $\Theta$  lines suggests the absence of the liquid phase and a direct transition from the gas to the crystalline phase for values of  $R > 30$ . The apparent similarities between the phase diagrams in the  $\Theta$  regime suggest that similar behavior in systems of larger sizes could be expected. The different order of the liquid-solid transition (first order for the 13mer and second order for the 30mer) is a consequence of the entropic character of the solid phase. For the 13mer, the icosahedron is the all-dominating morphology with comparatively low entropy and specific energy that sets apart the liquid phase and creates a phase-separation scenario. On the other hand, the “solid” phase of the 30mer is of rather highly entropic amorphous nature and allows for a continuous crossover from the liquid phase. In fact, given the small size of the system, the amorphous and the liquid phases are difficult to distinguish, though the transition is visible in the canonical quantities even at low  $R$  values (see Fig. 5).

It is instructive to consider the effects of the bond confinement range on the ground-state structures. It was previously shown [23] that a decrease in the interaction range of the Lennard-Jones potential can lead to the disappearance of icosahedral ground-state structures in “magic” system

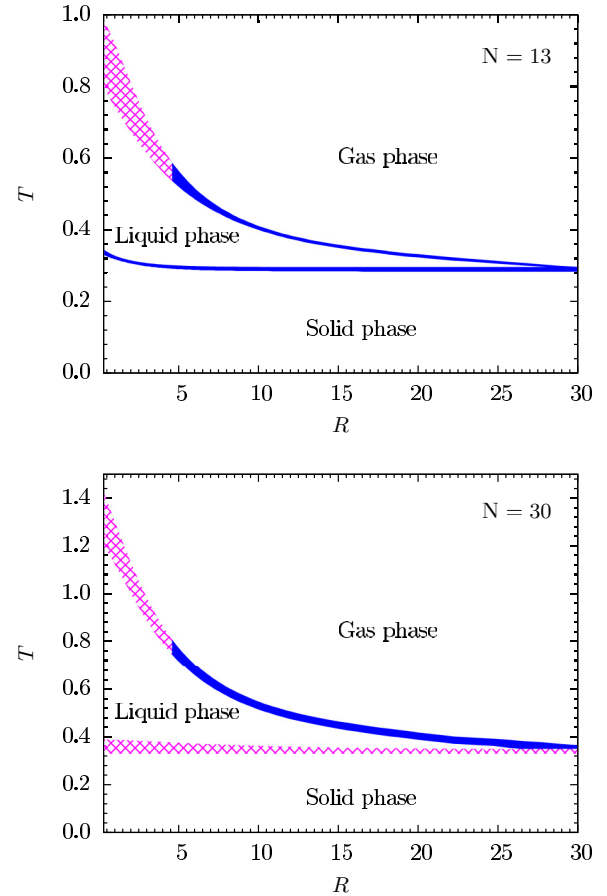


FIG. 7. (Color online) Structural phase diagrams for 13mers and 30mers, parametrized by the canonical temperature  $T$  and the confinement parameter  $R$ . The blue (solid) and pink (patterned) segments indicate first-order-like and second-order-like transitions, respectively.

sizes (such as  $N = 55$ ). In the present study, the ground-state energy of the 13mer remained virtually constant and the structures retained their icosahedral geometry even for extremely high values of the parameter  $R$ . This suggests that the low-temperature behavior of flexible homopolymer chains is dominated by the Lennard-Jones interactions while the FENE potential influences only the particular orderings of monomers within the ground-state structures. However, even this limited influence of the FENE potential has been shown to lead to significant effects such as the suppression of conformations with anti-Mackay, i.e., hcp-like overlayer [1].

## B. Microcanonical results

As discussed in the previous section, the results obtained by means of canonical analysis suggest that the  $\Theta$  transition acquires first-order-like character in systems with large confinement range. However, the analysis of structural transitions based on canonical quantities is often ambiguous. Canonical energy histograms are useful for determining the order of a transition only if their shape is clearly bimodal or unimodal. In this section, we turn to microcanonical analysis which offers a robust and unambiguous approach to the classification of structural transitions by means of

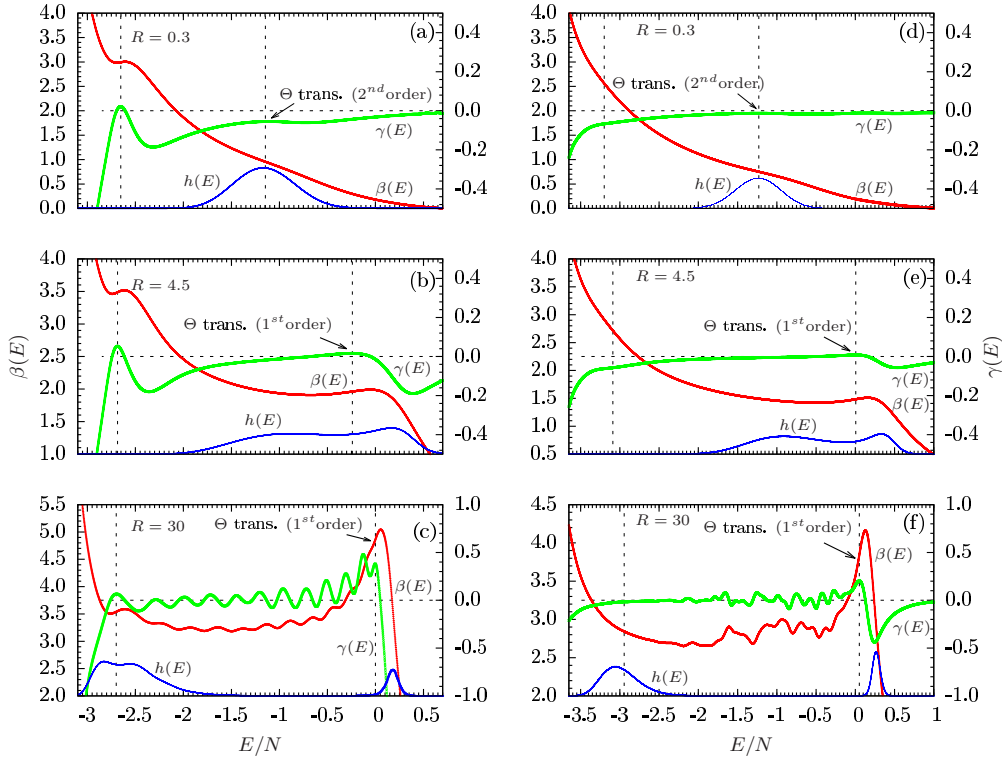


FIG. 8. (Color online) Microcanonical results for 13mers with bond confinement ranges (a)  $R = 0.3$ , (b) 4.5, and (c) 30 as well as for 30mers [(d)–(f)]. Shown are inverse temperature curves  $\beta(E)$ , their first derivatives  $\gamma(E) = d\beta(E)/dE$ , and (on arbitrary scale) the energy histograms  $h(E)$  at the  $\Theta$  transition temperature. The horizontal dashed line marks  $\gamma = 0$ . The positive valued peaks of  $\gamma(E)$  for values of  $R > 4.5$  clearly indicate that the  $\Theta$  transition is first order but remains separate from the freezing transition. The absorption of the freezing transition by the  $\Theta$  transition is apparent for large confinement ranges (c) and (f).

inflection-point analysis [2,60,65]. Figure 8 summarizes the results for chains of lengths with  $N = 13$  and 30 beads for values  $R = 0.3, 4.5, 30.0$ . In addition to the microcanonical temperature  $\beta(E)$  and its first derivative  $\gamma(E) = d\beta/dE$ , we also plot the canonical energy histograms  $h(E)$  obtained at the transition temperature.

For  $R = 0.3$ , the negative valued peaks of  $\gamma(E)$  indicate that the  $\Theta$  transition is of second order, in agreement with the observation that the canonical energy histograms for both system sizes are clearly unimodal. At  $R = 4.5$ , the peaks of  $\gamma(E)$  become positive and we conclude that the  $\Theta$  transition turns to first order. The signals for freezing transitions remain well outside of the back-bending region of the  $\Theta$  transition, confirming that the two transitions are well separated.

In the case  $R = 30$ , the multiple peaks in  $\gamma(E)$  indicate that the  $\Theta$  transition consists of a hierarchy of subphase transitions. This is particularly apparent in nucleation transitions with entropy reduction due to stepwise loss of translational entropy. Prominent examples are aggregation transitions in systems consisting of multiple polymer chains [2,39–41]. The system undergoes a direct transition from the solid phase into the gas phase through a series of subphase transitions consisting of individual monomers breaking away from the bulk. This can be seen nicely in Fig. 8(c), where a distinct hierarchy of subphase transitions for the 13mer with bond elasticity  $R = 30$  is noticeable. For the 30mer, at the same  $R$  value [Fig. 8(f)], subphases overlap to an extent that only an accumulated effect upon  $\beta(E)$  is visible.

The freezing transition is no longer an autonomous transition but instead becomes one of the subphase transitions that make up the  $\Theta$  transition. Eventually, this entails the absence of a separate liquid phase, which is in agreement with the overall picture obtained by the canonical analysis of fluctuating quantities.

The maximum  $R$  value is, of course, limited by the boundary of the simulation sphere that represents a steric constraint. The presence and the stability of the individual structural phases depend on the particle density. In the scenario presented here, where we investigate the disappearance of the liquid phase, we fixed the density to 0.001 particles per unit volume, whereas additional simulations at a 10 times larger density showed that the liquid phase remained stable, even for bond confinement ranges as large as  $R = 100$  (results not shown). In the unconstrained case of open boundaries (which for fixed particle number means vanishing density) and  $R \rightarrow \infty$ , both the liquid and solid phases are supposed to disappear and the gas phase would remain as the only stable phase. The disappearance of phases by reducing confinement was already observed in atomic cluster systems some time ago [44,45].

In Tables I and II, we have listed the microcanonical transition temperatures  $T_{f,\theta}$  and latent-heat values per monomer  $\Delta q_{f,\theta}$  for 13mers and 30mers with different bond confinement ranges  $R$ . Transition temperatures for the second-order transitions were obtained by microcanonical inflection-point analysis, whereas the transition points and latent heat

TABLE I. Microcanonical transition temperatures  $T_{f,\theta}$  and latent heats  $\Delta q_{f,\theta}$  at the freezing and  $\Theta$  transition points, respectively, for 13mers with different bond confinement ranges  $R$ .

$R$	$T_f$	$T_\theta$	$\Delta q_f$	$\Delta q_\theta$
0.3	$0.334 \pm 0.005$	$1.1 \pm 0.1$	$0.157 \pm 0.002$	N/A
1.5	$0.306 \pm 0.005$	$0.9 \pm 0.1$	$0.090 \pm 0.002$	N/A
3.0	$0.291 \pm 0.005$	$0.64 \pm 0.05$	$0.208 \pm 0.002$	N/A
4.5	$0.286 \pm 0.005$	$0.52 \pm 0.01$	$0.228 \pm 0.002$	$1.132 \pm 0.005$
9.0	$0.283 \pm 0.005$	$0.387 \pm 0.005$	$0.249 \pm 0.002$	$2.133 \pm 0.002$
15.0	$0.282 \pm 0.005$	$0.331 \pm 0.005$	$0.254 \pm 0.002$	$2.485 \pm 0.002$
30.0	$0.282 \pm 0.005$	$0.284 \pm 0.005$	$0.285 \pm 0.002$	$2.978 \pm 0.002$

values were estimated by means of microcanonical Maxwell construction (for descriptions of both methods, see, e.g., Ref. [2]).

#### IV. SUMMARY

In this study, we have investigated the thermodynamic behavior of a linear chain of beads connected by confined bonds which resembles a polymer for a large range of values of the bond confinement range  $R$ . Advanced parallel replica-exchange Monte Carlo methods, such as the MGME, were utilized in order to overcome the computational difficulties posed by the strong first-order-like behavior associated with the  $\Theta$  transition at large  $R$  values. Using the results obtained from the specific heat and the thermal fluctuations of the radius of gyration, we have constructed and compared features of the structural hyperphase diagrams for 13mers and 30mers. For low and intermediate confinement ranges, three distinct structural phases separated by the freezing and the  $\Theta$  transitions can be identified, in agreement with the expected behavior. With increasing values of the parameter  $R$ , however, the  $\Theta$  transition line shifts to lower temperatures and eventually merges with the freezing transition line, suggesting the absence of an independent liquid phase. Microcanonical inflection-point analysis provides conclusive evidence that the  $\Theta$  transition turns from second order to first order if the

TABLE II. Same as Table I, but for 30mers.

$R$	$T_f$	$T_\theta$	$\Delta q_f$	$\Delta q_\theta$
0.3	$0.39 \pm 0.01$	$1.3 \pm 0.1$	N/A	N/A
1.5	$0.39 \pm 0.01$	$1.2 \pm 0.1$	N/A	N/A
3.0	$0.38 \pm 0.01$	$0.88 \pm 0.05$	N/A	N/A
4.5	$0.37 \pm 0.01$	$0.69 \pm 0.01$	N/A	$1.650 \pm 0.005$
9.0	$0.36 \pm 0.01$	$0.496 \pm 0.005$	N/A	$2.647 \pm 0.002$
15.0	$0.35 \pm 0.01$	$0.416 \pm 0.005$	N/A	$3.057 \pm 0.002$
30.0	$0.35 \pm 0.01$	$0.344 \pm 0.005$	N/A	$3.399 \pm 0.002$

bond confinement range parameter  $R$  exceeds a threshold value. This change in the character of the  $\Theta$  transition is not influenced by the freezing transition, which in this part of the phase diagram is still well separated from the  $\Theta$  point. Increasing the confinement range further,  $\Theta$  and freezing transitions merge and exhibit clear indications of a hierarchical nucleation transition. In this regime, the beads are quasifree and interact likewise with others, bonded or nonbonded. The still coupled system behaves like an atomic cluster in a dilute regime. The general structure of the hyperphase diagrams can be expected to remain qualitatively intact even for substantially larger systems. The only anticipated change is that the freezing transition is of first order for all system sizes with more than about 40 monomers [65].

Our systematic study covers the technologically and biologically interesting regime of polymer chains with bond elasticities ranging from stiff to highly elastic, which includes all realistic linear macromolecules, and extends into the space of confined systems that behave like atomic clusters. Since our results are supposed to be generic, they allow for a classification of the expected transition behavior on the basis of the effective bond confinement range of these systems.

#### ACKNOWLEDGMENTS

This work has been supported partially by the NSF under Grant No. DMR-1207437 and by CNPq (National Council for Scientific and Technological Development, Brazil) under Grant No.402091/2012-4.

- [1] S. Schnabel, M. Bachmann, and W. Janke, *J. Chem. Phys.* **131**, 124904 (2009).
- [2] M. Bachmann, *Thermodynamics and Statistical Mechanics of Macromolecular Systems* (Cambridge University Press, Cambridge, 2014).
- [3] K. F. Lau and K. A. Dill, *Macromolecules* **22**, 3986 (1989).
- [4] F. H. Stillinger, T. Head-Gordon, and C. L. Hirshfeld, *Phys. Rev. E* **48**, 1469 (1993).
- [5] F. H. Stillinger and T. Head-Gordon, *Phys. Rev. E* **52**, 2872 (1995).
- [6] A. Irbäck, C. Peterson, F. Potthast, and O. Sommelius, *J. Chem. Phys.* **107**, 273 (1997).
- [7] H.-P. Hsu, V. Mehra, W. Nadler, and P. Grassberger, *J. Chem. Phys.* **118**, 444 (2003).
- [8] M. Bachmann and W. Janke, *Phys. Rev. Lett.* **91**, 208105 (2003).
- [9] M. Bachmann and W. Janke, *J. Chem. Phys.* **120**, 6779 (2004).
- [10] M. Bachmann, H. Arkin, and W. Janke, *Phys. Rev. E* **71**, 031906 (2005).
- [11] S. Schnabel, M. Bachmann, and W. Janke, *Phys. Rev. Lett.* **98**, 048103 (2007).
- [12] S. Schnabel, M. Bachmann, and W. Janke, *J. Chem. Phys.* **126**, 105102 (2007).
- [13] I. Carmesin and K. Kremer, *Macromolecules* **21**, 2819 (1988).
- [14] H. P. Deutsch and K. Binder, *J. Chem. Phys.* **94**, 2294 (1991).
- [15] P. Grassberger, *Phys. Rev. E* **56**, 3682 (1997).
- [16] T. Vogel, M. Bachmann, and W. Janke, *Phys. Rev. E* **76**, 061803 (2007).
- [17] W. Paul, T. Strauch, F. Rampf, and K. Binder, *Phys. Rev. E* **75**, 060801(R) (2007).

- [18] S. Schnabel, T. Vogel, M. Bachmann, and W. Janke, *Chem. Phys. Lett.* **476**, 201 (2009).
- [19] M. P. Taylor, W. Paul, and K. Binder, *J. Chem. Phys.* **131**, 114907 (2009).
- [20] M. P. Taylor, W. Paul, and K. Binder, *Phys. Rev. E* **79**, 050801(R) (2009).
- [21] D. T. Seaton, T. Wüst, and D. P. Landau, *Phys. Rev. E* **81**, 011802 (2010).
- [22] D. T. Seaton, S. Schnabel, D. P. Landau, and M. Bachmann, *Phys. Rev. Lett.* **110**, 028103 (2013).
- [23] J. Gross, T. Neuhaus, T. Vogel, and M. Bachmann, *J. Chem. Phys.* **138**, 074905 (2013).
- [24] M. Bachmann and W. Janke, *Phys. Rev. Lett.* **95**, 058102 (2005).
- [25] J. Krawczyk, T. Prellberg, A. L. Owczarek, and A. Rechnitzer, *Europhys. Lett.* **70**, 726 (2005).
- [26] M. Bachmann and W. Janke, *Phys. Rev. E* **73**, 041802 (2006).
- [27] M. Bachmann and W. Janke, *Phys. Rev. E* **73**, 020901(R) (2006).
- [28] J. Luettmer-Strathmann, F. Rampf, W. Paul, and K. Binder, *J. Chem. Phys.* **128**, 064903 (2008).
- [29] M. Möddel, M. Bachmann, and W. Janke, *J. Phys. Chem. B* **113**, 3314 (2009).
- [30] L. Wang, T. Chen, X. Lin, Y. Liu, and H. Liang, *J. Chem. Phys.* **131**, 244902 (2009).
- [31] A. D. Swetnam and M. P. Allen, *Phys. Chem. Chem. Phys.* **11**, 2046 (2009).
- [32] M. Möddel, W. Janke, and M. Bachmann, *Phys. Chem. Chem. Phys.* **12**, 11548 (2010).
- [33] T. Vogel and M. Bachmann, *Phys. Rev. Lett.* **104**, 198302 (2010).
- [34] M. Möddel, W. Janke, and M. Bachmann, *Macromolecules* **44**, 9013 (2011).
- [35] Y. W. Li, T. Wüst, and D. P. Landau, *Phys. Rev. E* **87**, 012706 (2013).
- [36] M. Möddel, W. Janke, and M. Bachmann, *Phys. Rev. Lett.* **112**, 148303 (2014).
- [37] T. Vogel, J. Gross, and M. Bachmann, *J. Chem. Phys.* **142**, 104901 (2015).
- [38] C. Junghans, M. Bachmann, and W. Janke, *Phys. Rev. Lett.* **97**, 218103 (2006).
- [39] C. Junghans, M. Bachmann, and W. Janke, *J. Chem. Phys.* **128**, 085103 (2008).
- [40] C. Junghans, M. Bachmann, and W. Janke, *Europhys. Lett.* **87**, 40002 (2009).
- [41] C. Junghans, W. Janke, and M. Bachmann, *Comp. Phys. Commun.* **182**, 1937 (2011).
- [42] J. P. K. Doye, D. J. Wales, and R. S. Berry, *J. Chem. Phys.* **103**, 4234 (1995).
- [43] J. P. K. Doye and D. J. Wales, *J. Phys. B* **29**, 4859 (1996).
- [44] J. P. Neirotti, F. Calvo, D. L. Freeman, and J. D. Doll, *J. Chem. Phys.* **112**, 10340 (2000).
- [45] F. Calvo, J. P. Neirotti, D. L. Freeman, and J. D. Doll, *J. Chem. Phys.* **112**, 10350 (2000).
- [46] P. A. Frantsuzov and V. A. Mandelshtam, *Phys. Rev. E* **72**, 037102 (2005).
- [47] L. Cheng and J. Yang, *J. Phys. Chem. A* **111**, 5287 (2007).
- [48] F. Calvo, J. P. K. Doye, and D. J. Wales, *J. Chem. Phys.* **116**, 2642 (2002).
- [49] R. H. Swendsen and J.-S. Wang, *Phys. Rev. Lett.* **57**, 2607 (1986).
- [50] K. Hukushima and K. Nemoto, *J. Phys. Soc. Jpn.* **65**, 1604 (1996).
- [51] K. Hukushima, H. Takayama, and K. Nemoto, *Int. J. Mod. Phys. C* **7**, 337 (1996).
- [52] C. J. Geyer, in *Computing Science and Statistics, Proceedings of the 23rd Symposium on the Interface*, edited by E. M. Keramidas (Interface Foundation, Fairfax Station, 1991), p. 156.
- [53] E. Marinari and G. Parisi, *Europhys. Lett.* **19**, 451 (1992).
- [54] A. P. Lyubartsev, A. A. Martsinovski, S. V. Shevkunov, and P. N. Vorontsov-Velyaminov, *J. Chem. Phys.* **96**, 1776 (1992).
- [55] B. A. Berg and T. Neuhaus, *Phys. Lett. B* **267**, 249 (1991).
- [56] B. A. Berg and T. Neuhaus, *Phys. Rev. Lett.* **68**, 9 (1992).
- [57] W. Janke, *Physica A* **254**, 164 (1998).
- [58] B. A. Berg, *Comp. Phys. Commun.* **153**, 397 (2003).
- [59] B. A. Berg, *Markov Chain Monte Carlo Simulations* (World Scientific, Singapore, 2004).
- [60] M. Bachmann, *Phys. Scr.* **87**, 058504 (2013).
- [61] F. Wang and D. P. Landau, *Phys. Rev. Lett.* **86**, 2050 (2001).
- [62] F. Wang and D. P. Landau, *Phys. Rev. E* **64**, 056101 (2001).
- [63] T. Vogel, Y. W. Li, T. Wüst, and D. P. Landau, *Phys. Rev. Lett.* **110**, 210603 (2013).
- [64] M. N. Rosenbluth and A. W. Rosenbluth, *J. Chem. Phys.* **23**, 356 (1955).
- [65] S. Schnabel, D. T. Seaton, D. P. Landau, and M. Bachmann, *Phys. Rev. E* **84**, 011127 (2011).
- [66] D. H. E. Gross, *Microcanonical Thermodynamics* (World Scientific, Singapore, 2001).
- [67] K. Qi and M. Bachmann, *J. Chem. Phys.* **141**, 074101 (2014).
- [68] M. E. Fisher, *Rep. Prog. Phys.* **30**, 615 (1967).
- [69] M. P. Taylor, P. P. Aung, and W. Paul, *Phys. Rev. E* **88**, 012604 (2013).
- [70] J. C. S. Rocha, S. Schnabel, D. P. Landau, and M. Bachmann, *Phys. Rev. E* **90**, 022601 (2014).
- [71] M. P. Taylor and J. Luettmer-Strathmann, *J. Chem. Phys.* **141**, 204906 (2014).
- [72] T. Neuhaus and J. S. Hager, *Phys. Rev. E* **74**, 036702 (2006).
- [73] R. B. Bird, C. F. Curtiss, R. C. Armstrong, and O. Hassager, *Dynamics of Polymeric Liquids*, 2nd ed. (Wiley, New York, 1987).
- [74] K. Kremer and G. S. Grest, *J. Chem. Phys.* **92**, 5057 (1990).
- [75] A. Milchev, A. Bhattacharya, and K. Binder, *Macromolecules* **34**, 1881 (2001).
- [76] A. M. Ferrenberg and R. H. Swendsen, *Phys. Rev. Lett.* **63**, 1195 (1989).
- [77] S. Kumar, J. M. Rosenberg, D. Bouzida, R. H. Swendsen, and P. A. Kollman, *J. Comput. Chem.* **13**, 1011 (1992).
- [78] I. M. Lifshitz, A. Yu. Grosberg, and A. R. Khokhlov, *Rev. Mod. Phys.* **50**, 683 (1978).
- [79] A. R. Khokhlov, *Physica A* **105**, 357 (1981).
- [80] D. D. Frantz, *J. Chem. Phys.* **115**, 6136 (2001).
- [81] V. A. Mandelshtam and P. A. Frantsuzov, *J. Chem. Phys.* **124**, 204511 (2006).